



OPEN

Magnetic resonance imaging of tumor response to stroma-modifying pegvorhialuronidase alpha (PEGPH20) therapy in early-phase clinical trials

Andrés M. Arias-Lorza¹, James R. Costello², Sunil R. Hingorani^{3,4}, Daniel D. Von Hoff^{5,6}, Ronald L. Korn⁷ & Natarajan Raghunand^{1,8}✉

Pre-clinical and clinical studies have shown that PEGPH20 depletes intratumoral hyaluronic acid (HA), which is linked to high interstitial fluid pressures and poor distribution of chemotherapies. 29 patients with metastatic advanced solid tumors received quantitative magnetic resonance imaging (qMRI) in 3 prospective clinical trials of PEGPH20: HALO-109-101 (NCT00834704), HALO-109-102 (NCT01170897), and HALO-109-201 (NCT01453153). Apparent Diffusion Coefficient of water (ADC), T1, k^{trans} , v_{pr} , v_{er} and iAUC maps were computed from qMRI acquired at baseline and ≥ 1 time point post-PEGPH20. Tumor ADC and T1 decreased, while iAUC, k^{trans} , v_{pr} and v_e increased, on day 1 post-PEGPH20 relative to baseline values. This is consistent with HA depletion leading to a decrease in tumor extracellular water content and an increase in perfusion, permeability, extracellular matrix space, and vascularity. Baseline parameter values predictive of pharmacodynamic responses were: ADC $> 1.46 \times 10^{-3} \text{ mm}^2/\text{s}$ (Balanced Accuracy (BA) = 72%, $p < 0.01$), T1 $> 0.54 \text{ s}$ (BA = 82%, $p < 0.01$), iAUC $< 9.2 \text{ mM}\cdot\text{s}$ (BA = 76%, $p < 0.05$), $k^{trans} < 0.07 \text{ min}^{-1}$ (BA = 72%, $p = 0.2$), $v_e < 0.17$ (BA = 68%, $p < 0.01$), and $v_p < 0.02$ (BA = 60%, $p < 0.01$). A low v_e at baseline was moderately predictive of response in any parameter (BA = 65.6%, $p < 0.01$ averaged across patients). These qMRI biomarkers are potentially useful for guiding patient pre-selection and post-treatment follow-up in future clinical studies of PEGPH20 and other tumor stroma-modifying anti-cancer therapies.

Keywords Pegvorhialuronidase alpha, Hyaluronan, Cancer, Clinical trial, Magnetic resonance imaging

The extracellular matrix (ECM) of solid tumors can contain significant amounts of hyaluronan or hyaluronic acid (HA), a linear glycosaminoglycan with repeating disaccharide units of glucuronic acid and N-acetylglucosamine. HA binds up to 15 water molecules per disaccharide, forming a viscoelastic gel-fluid phase that has been mechanistically linked to high interstitial fluid pressure (IFP) in tumors. A dense ECM and high IFP, coupled with dysfunctional tumor microvasculature, leads to poor distribution into the tumor mass of systemically administered therapeutics¹⁻³. High tumor levels of HA can also promote intratumoral hypoxia and acidity⁴, further contributing to poorer prognoses. Therefore, targeting HA in the ECM of tumors with high HA accumulation is therapeutically relevant.

¹Department of Cancer Physiology, Moffitt Cancer Center, Tampa, FL, USA. ²Department of Radiology, Moffitt Cancer Center, Tampa, FL, USA. ³Division of Hematology and Oncology, Department of Medicine, University of Nebraska Medical Center, Omaha, NE, USA. ⁴Fred & Pamela Buffett Cancer Center, Pancreatic Cancer Center of Excellence, University of Nebraska Medical Center, Omaha, NE, USA. ⁵Translational Genomics Research Institute (TGen), Scottsdale, AZ, USA. ⁶HonorHealth Clinical Research Institute, Phoenix, AZ, USA. ⁷Imaging Endpoints Core Lab, Scottsdale, AZ, USA. ⁸Department of Oncologic Sciences, University of South Florida, Tampa, FL, USA. ✉email: Natarajan.Raghunand@moffitt.org

Pegvorhialuronidase alpha (PEGPH20) represents an investigational anticancer therapeutic that was developed to target and degrade tumor HA^{5,6}. In vitro and preclinical studies have shown that PEGPH20 depletes HA, leading to decreased IFP, increased perfusion, decreased water, increased micro-vessel area, reduced hypoxia, increased pH, and changes in water diffusion, among other therapeutic events in tumor^{2,4,7–9}. Tumor growth inhibition and improved survival^{10,11}, and an increase in the intra-tumoral concentration of concomitant chemotherapies^{7,9}, following PEGPH20 has been reported in multiple mouse models.

These results led to the clinical development and testing of PEGPH20. Early phase clinical studies showed a decrease in tumor HA and an increase in tumor perfusion resulting in increased survival in patients with high tumor HA receiving PEGPH20 in combination with the chemotherapy drug gemcitabine (GEM)^{5,6,12,13}. In a phase 1b study of metastatic pancreatic ductal adenocarcinoma (PDA), stratification of patients for baseline tumor HA content indicated that median progression-free survival (PFS) and overall survival (OS) were longer in patients with high HA tumors than in those with low HA tumors⁶. In a randomized phase II study of PEGPH20 plus nab-paclitaxel/GEM (PAG) vs. nab-paclitaxel/GEM (AG), in patients with high intratumoral HA, the objective response rate was 45% and median overall survival was 11.5 months in patients who received PAG, compared with 31% and 8.5 months in patients who received AG¹³. Based on results from the Phase 1b and Phase II studies, a randomized, double-blind phase III study of PEGPH20 + AG vs. placebo + AG was conducted in patients with high-HA metastatic PDA (HALO-109-301, NCT02715804). Results from 492 patients indicated that the addition of PEGPH20 to AG increased the objective response rate (ORR) but did not improve the duration of response, OS, or PFS¹⁴. In another phase II study of metastatic PDA, patients with unknown tumor HA status were randomly assigned to receive either the combination of mFOLFIRINOX plus PEGPH20 or mFOLFIRINOX alone (n = 138). The combination with PEGPH20 was less tolerated and increased the likelihood of missed doses¹⁵. With similar obstacles encountered with other agents targeting tumor stroma in PDA (reviewed in¹⁶), targeting desmoplasia alone appears insufficient, and other properties such as lack of significant neoantigens, low tumor mutational burden, and epithelial-to-mesenchymal transition are hypothesized to play a role¹⁷. Another confounding factor may be that the tumor stroma, though a physical barrier hampering drug delivery, may also have protective effects in restraining tumor growth and progression¹⁵. Continued clinical development of PEGPH20 has been halted, and a need for additional pre-clinical and retrospective analyses is indicated to improve our understanding of the failures of tumor stroma remodeling as a therapeutic strategy¹⁴.

A clear need is development of criteria for selecting patients who are likely to benefit from the addition of PEGPH20 to their therapeutic regimen. Tumor HA status on biopsy-based immunohistochemical scoring may be inadequate for prognostication¹⁸. Biopsy-based assays are invasive and cannot capture intratumoral spatial heterogeneity or inter-lesion heterogeneity in oligometastatic disease¹⁹ as was the case in HALO-109-301¹⁴. Radiologic imaging can provide non-invasive longitudinal assessment of tumor heterogeneity over the entire 3D volumes of multiple tumors in a patient. For example, Apparent Diffusion Coefficient (ADC) estimated from Diffusion Weighted (DW)-MRI provides a non-invasive measure of tumor water content and mobility, both properties reported to be affected by PEGPH20^{8,20–22}. Tumor perfusion and microvascular permeability (k^{trans}) calculated from Dynamic Contrast-Enhanced (DCE)-MRI has been reported to increase following PEGPH20 in pre-clinical and clinical studies^{5,6,9}.

Here we report the first complete analysis of DW-MRI and DCE-MRI collected in three early-phase clinical trials of PEGPH20 (HALO-109-101, HALO-109-102, and HALO-109-201). On a relatively large sample of patients with advanced solid tumors, we computed maps of ADC, T1, k^{trans} , plasma volume fraction (v_p), extracellular extravascular volume fraction (v_e), and Area-Under-the-Gadolinium-Concentration-Curve-at-90 s (iAUC). We report both early post-PEGPH20 prognostic, and pre-PEGPH20 predictive, biomarkers that could be used to select patients who are good candidates for PEGPH20 therapy.

Methods

Clinical and MRI study design

We collected MRI data in three clinical trials of PEGPH20: HALO-109-101 (NCT00834704), HALO-109-102 (NCT01170897), and HALO-109-201 (NCT01453153). The studies were conducted at five centers in the United States and four centers in Russia in accordance with the Declaration of Helsinki and Good Clinical Practice Guidelines of the International Conference on Harmonization, and was approved by the local institutional review board at each study site. Written informed consent was obtained from all patients. In all studies, eligible patients were at least 18 years of age. In HALO-109-101 and HALO-109-102, eligible patients had diagnoses of pathologically confirmed, measurable, metastatic or locally advanced solid tumors refractory to standard treatment⁵. In HALO-109-201, eligible patients had a Karnofsky score of $\geq 70\%$ and a life expectancy of at least 3 months with newly diagnosed, previously untreated, histologically confirmed stage IV PDA and documented metastasis to the liver and/or lung⁶.

HALO-109-101 was a Phase I dose-escalation study (0.5–50 $\mu\text{g}/\text{kg}$) on 14 patients, with PEGPH20 administered once or twice weekly on day 1 (and 4) of each 21 day cycle⁵. Baseline HA staining was obtained in 7 subjects. DW-MRI was obtained in 12 subjects, 10 with imaging done both before and 2–4 days after PEGPH20.

In HALO-109-102, PEGPH20 was administered (0.5–5 $\mu\text{g}/\text{kg}$) once or twice weekly on day 1 (and 4) in 25 day cycles together with the anti-inflammatory dexamethasone administered one hour before PEGPH20 in 26 subjects⁵. HA staining before and after drug (day 2 or beyond) was available in 6 patients. DW-MRI was obtained in 16 subjects, of whom 13 subjects had available DW-MRI at baseline and following PEGPH20 (day 1; days 2, 3 or 4, and end of first cycle). On the same dates, pre-contrast T1-weighted (T1w)-MRI and DCE-MRI were obtained in 16 subjects, of whom 13 subjects had imaging available at baseline and following PEGPH20.

In HALO-109-201, 28 subjects received escalating intravenous doses of PEGPH20 (1, 1.6, 3 $\mu\text{g}/\text{kg}$) in combination with GEM (1,000 mg/m^2 i.v.; Sun Pharmaceuticals) using a standard 3 + 3 dose-escalation design. In

cycle 1 (8 weeks), PEGPH20 was administrated twice weekly (days 1 and 4) for 4 weeks, then once weekly for 3 weeks. GEM was administrated 24 h after the first dose of PEGPH20, and all other doses were given 2 to 24 h after PEGPH20 once weekly for 7 weeks, followed by 1 week off treatment. In each subsequent 4-week cycle, PEGPH20 and GEM were administered once weekly for 3 weeks, followed by 1 week off. Dexamethasone (8 mg) was given 1 h before and 8–12 h after PEGPH20 administration. Twenty patients had a baseline biopsy assessed for HA content⁶. Pre-contrast T1w-MRI and DCE-MRI series were obtained before the first dosing on day 1 of week 1 in addition to 8 and/or 24 h after the first dose of PEGPH20 in Cycle 1, and then 24 h after the last dose of PEGPH20 in Cycle 1 (Week 7). 7 subjects were imaged, with 6 of these subjects having imaging available at baseline and following PEGPH20. A CONSORT diagram is shown in Supplementary Fig. 1.

Tumor HA immunohistochemistry

On available tumor biopsies, degree of positivity for HA was semi-quantified using either a pathologist visual scoring method (H-score) or digital image analysis (HA%)^{5,6}. Biopsies of tumors visible on qMRI could be analyzed for correlation with their qMRI parameters (see Table 1).

MRI acquisition

Single-shot EPI DW-MRI images were acquired with typically 20 slices reconstructed to a matrix size of 256 × 256, in-plane resolution of ~1.5 × 1.5 mm², slice thickness of 8 mm, TR ~6 s, TE ~80 ms, field strength 1.5 T, FA 90°, and *b* values of 0 and 450 s/mm². Typically, 3 replicates of the DW-MRI were obtained per session. As part of the scanner qualification process, each participating imaging site was shipped a DW-MRI phantom comprising an inner sealed 50 mL tube containing distilled water that was cemented to the inside of the lid of an empty

	Patient ID	Dose level (µg/Kg)	Primary cancer	HA staining ²	Response ³	Lesions on DW-MRI	Lesions on T1w-MRI	Lesions on DCE-MRI
HALO-109-101	101-001-109	0.75	Ovarian	–	SD	1	0	0
	101-002-102	50	CRC	–	PD	1	0	0
	101-002-106	0.5	CRC	–	PD	1	0	0
	101-002-114	1.5	Prostate	–	PD	1	0	0
	101-003-103	0.5	CRC	–	AE	8	0	0
	101-003-104	0.5	Pancreas	10%,0,150 → –	PD	1	0	0
	101-003-105	0.5	Bladder	–	PD	3	0	0
	101-003-108	0.75	Carcinoid	–	PD	5	0	0
	101-003-110	0.75	CRC	–	PD	1	0	0
	102-003-112	1	NSCLC	–	PD	1	0	0
HALO-109-102	102-002-102	1.6	Esophageal	–	PD	1	0	1
	102-002-103	5	NSCLC	–	AE	0	1	1
	102-002-113	3	Pancreas	–	AE	1	1	1
	102-002-115	3	Pancreas	–	AE	1	1	1
	102-002-126	3	CRC	–	SD	1	1	1
	102-003-104	1.6	CRC	T2: 17.9%, – ,- → 3.5%, –,-	PD	2	2	2
	102-003-105	1.6	CRC	–	PD	5	2	2
	102-003-117	3	CRC	12.2%, –,- → 20.8%, – ,-	PD	1	1	1
	102-003-118	3	Tonsil	–	PD	1	1	1
	102-005-111	3	CRC	–	AE	1	1	1
	102-006-107	3	Pancreas	–	PD	1	1	1
	102-006-110	3	CRC	–	AE	1	1	1
	102-006-124	3	CRC	–	PD	1	1	1
HALO-109-201	201-001-301	3	Pancreas	–,280,270 → –		PR	0	1
	201-001-304	3	Pancreas	–	PR	0	1	1
	201-003-306	3	Pancreas	–	SD	0	1	1
	201-007-405	3	Pancreas	T1: –,40,260 → –,15,150	PR	0	3	5
	201-007-409	3	Pancreas	–,100,240 → –	PR	0	1	1
	201-007-414	3	Pancreas	T1: –,30,190 → –	PR	0	5	5
	# Patients: 29				# Lesions:	40	26	29

Table 1. Summary of patient data. ¹CRC: Colorectal Cancer, NSCLC: Non-small-cell lung carcinoma. ²Tumor biopsied (in case of multiple tumors): HA%, tumor, and stroma H-score before and after PEGPH20. ³Response by RECIST. SD: Stable Disease, PD: Progressive Disease, PR: Partial Response, AE: discontinuation of the study due to Adverse Events.

outer jar. Sites were instructed to fill the outer jar with crushed ice and cold tap water, screw on the lid with the inner tube, and wait > 20 min prior to loading the phantom into the scanner, following the method of Chenevert and colleagues^{23,24}. Sites were instructed to acquire DW-MRI with $b = 0, 450, 500, 800, 1000,$ and 2000 s/mm^2 , repeated 3 times. Phantom images were analyzed qualitatively for geometric distortions and quantitatively after mono-exponential fitting for ADC (Supplementary Fig. 2).

Pre-contrast 3D Gradient Echo (3D-GRE) T1w-MRI images were acquired with typically 12 slices reconstructed to a matrix size of 256×256 , in-plane resolution of $\sim 1.3 \times 1.3 \text{ mm}^2$, slice thickness of $\sim 5 \text{ mm}$, TR $\sim 3 \text{ ms}$, TE $\sim 1 \text{ ms}$, field strength 1.5 T, and FA = $15^\circ, 23^\circ, 30^\circ,$ and 60° . The DCE-MRI series comprised of > 40 3D-GRE T1w-MRI repeats acquired every $\sim 8 \text{ s}$ with the same parameters as the pre-contrast T1w images but with a fixed FA = 30° . Gadolinium contrast (0.1 mmol/kg) was power-injected at 4 mL/s after 4–10 repeats had been collected in the T1w dynamic series, and chased with 20 mL saline at 4 mL/s.

Image post-processing

All DW-MRI images per session were co-registered, and ADC was computed per replicate using the mono-exponential model²⁵. A mean ADC per session was obtained by averaging the available ADC replicates.

Pre-contrast T1w-MRI images acquired with multiple FA and the DCE-MRI series were co-registered per session²⁵. T1 relaxation time maps were calculated by fitting the T1w image intensities to the GRE signal equation while enforcing spatial smoothness in T1 maps²⁶. In case of noticeable intensity inhomogeneity at the tumor site, true FA in the images were estimated before getting T1 maps²⁷. Also, in case of differences in intensity scaling between T1w-MRI images, the scaling factors were estimated prior to computing T1 maps²⁵. Gadolinium concentration maps were calculated from the change in pixel-wise T1 relative to pre-contrast T1 in the DCE-MRI series using the published relaxivity at the relevant field strength of the contrast agent used in a given patient²⁸. In some cases, pre-contrast T1w-MRI images were not available or had not been acquired according to the study protocol. In these cases, reference values of T1 were used for normal tissues and/or blood. iAUC maps were computed as the area-under-the-gadolinium-concentration-curve 90 s after contrast injection. To describe the contrast exchange between blood and tissue we used the extended Tofts model to obtain $k^{trans}, v_p,$ and v_e . The Arterial Input Function (AIF) was obtained by averaging selected contrast curves in pixels in a main artery²⁵. Finally, all parameter maps including ADC were co-registered across scan dates. The MATLAB code implementation of the image pre-processing and per-patient HTML reports that depict all slices of raw qMRI images, processed qMRI images, and computed maps of ADC, T1, iAUC, $k^{trans}, v_p,$ and v_e , from all scan dates of each subject, have been publicly shared (*cf.* Data and Code Sharing Statement).

Segmentation

Study images were centrally collected at Imaging Endpoints Core Lab, and tumor and reference tissues were identified by central review. Target tumors and Volumes-of-Interest (VOIs) within normal reference tissues were then manually contoured in a blinded fashion by an experienced imaging scientist (NR) on both on DW-MRI and DCE-MRI for each visit. To evaluate robustness of tumor metrics to manual annotation, a subset of five patients were also annotated in a blinded manner by an experienced radiologist (JRC).

Statistical Analysis

MRI data were analyzed on VOI and pixelwise basis. In VOI analysis, median ADC, T1, iAUC, $k^{trans}, v_p,$ and v_e values within segmented VOIs were computed at each scan date. Following Quantitative Imaging Biomarkers Alliance (QIBA) recommendations²⁹, median parameter changes per visit are identified as significant changes if these are either above or below the Repeatability Coefficient (RC), where 95% of repeated measurements should be inside the $-RC + RC$ range. From the ADC replicates at baseline per patient and tumor, we obtained the median ADC Repeatability Coefficient ($RC = 2.77\sqrt{\sigma^2}$). For patients in whom multiple replicates of the DW-MRI were not available at the baseline scan date, the whole data RC was used instead. Replicate scans were not acquired for T1w-MRI or DCE-MRI; therefore, as recommended by QIBA, RC values were obtained from literature on similar data in tumors; RC = 0.27 s for T1³⁰, RC = 32% for iAUC, RC = -45% to 83% for k^{trans} , RC = 0.076 for v_e ³¹, and RC = 0.0062 for v_p ³². Tumors with a positive or negative (depending on the parameter) significant changes in a parameter were labeled pharmacodynamic responders (P), and otherwise labeled pharmacodynamic non-responders (N). Models to predict positive (PP) or negative (PN) tumor pharmacodynamic response were evaluated by their sensitivity = $(PP \cap P)/P$, specificity = $(PN \cap N)/N$, and Balanced Accuracy (BA) = $(\text{sensitivity} + \text{specificity})/2$. A similar assessment was performed for pixel-wise analysis of tumors from patients with available co-registered MRI sequences across scan dates.

Results

VOI analysis

Ten patients from HALO-109-101 and 13 patients from HALO-109-102 have DW-MRI available from multiple scan dates; however, in one patient ADC could not be computed as $b = 0 \text{ s/mm}^2$ images were not acquired. Thus, ADC of a total of 40 tumors in 22 patients were analyzed, out of which ADC replicates at baseline were available for 18 patients with a total of 28 tumors. At baseline, ADC from patient 101-003-103 was not included as the b values used for DW-MRI in this subject ($0 \text{ \& } 1000 \text{ s/mm}^2$) were a deviation from the prescribed study protocol values ($0 \text{ \& } 450 \text{ s/mm}^2$). Also, ADC at baseline for patient 102-002-113 could not be calculated as the $b = 0 \text{ s/mm}^2$ images were not acquired. Therefore, changes in ADC at baseline from 20 patients with a total of 31 tumors were analyzed. Further, 19 patients with multiple scan dates of T1w-MRI and DCE-MRI were available (13 from HALO-109-102 and 6 from HALO-109-201); however, in one patient from HALO-109-102 (patient 102-002-102) T1 maps could not be obtained as T1w-MRI were acquired using one FA only. Additionally two tumors

in patient 201-007-405 were not clearly visible on T1w-MRI. Therefore, T1 from 18 patients with a total of 26 tumors, and DCE parameters (iAUC, k^{trans} , v_p , and v_e) from 19 patients with a total of 29 tumors, were analyzed. Patient 102-003-104 did not have T1w-MRI images at baseline. Patients 102-003-104 and 102-003-117 were left out of the DCE-MRI analysis at baseline due to missing T1w-MRI and DCE images, respectively. Therefore, changes in T1 in 24 tumors from 17 patients and changes in DCE-MRI parameters in 26 tumors from 17 patients were analyzed. In total, 29 patients were analyzed, and a summary of patient data is described in Table 1. Drug pharmacokinetics and survival information per patient are described in Supplementary Table 1.

Figure 1 shows parameter maps per visit of patient 102-003-105 (tumor 2) with a colorectal cancer metastasis in the liver. At Day 1 following PEGPH20, a relatively uniform decrease in ADC and T1, and an increase in iAUC, k^{trans} , and v_e , within the tumor are observed. An increase in v_p is observed in a few pixels. Over the following days these parameters tended to return to baseline. Per-patient HTML reports that depict all slices of raw qMRI images, processed qMRI images, and computed maps of ADC, T1, iAUC, k^{trans} , v_p , and v_e , from all scan dates of each subject, have been publicly shared (cf. Data and Code Sharing Statement).

Median parameter changes in tumor are depicted in Figs. 2 and 3. Changes outside the Repeatability Coefficient (RC) range are also depicted, indicating significant differences with respect to baseline. A Bland–Altman plot of ADC depicting the measurement variability described by RC for 28 tumors from 18 patients with available ADC replicates at baseline is shown in Fig. 2a. For the remaining 3 (= 31–28) tumors, we applied the whole data RC = $0.8 \times 10^{-3} \text{ mm}^2/\text{s}$. In the 31 tumors that were analyzable, a decrease in ADC on day 1 relative to baseline was observed in 24 tumors, 8 tumors were below –RC, 2 tumors above +RC, and the remaining did not have a significant change. In the next visit, ADC of 6 out of 16 tumors were below –RC and of 1 tumor was above +RC. In the last visit, ADC of two and one out of 9 tumors were below –RC and above +RC respectively (Fig. 2b).

On day 1 relative to baseline, tumor T1 decreased below –RC in 13 out of 24 tumors, and increased above +RC in 2 tumors. At the next visit, the corresponding numbers were 5 tumors below –RC and 4 tumors above +RC, out of 22 total evaluable tumors. In the last visit, T1 of 1 each of 7 tumors were below –RC and above +RC (Fig. 2c).

On Day 1 relative to baseline, 3 and 10 out of 26 tumors exhibited tumor iAUC changes that were below –RC and above +RC respectively. At the following visits, tumor iAUC of 8 and 3 out of 24 tumors, and 5 and 0 out of 6 tumors, were below –RC and above +RC (Fig. 2d).

Tumor k^{trans} of 0 and 9 tumors on day 1, 2 and 3 tumors on visit 2, and 4 and 0 tumors in the last visit, were below –RC and above +RC respectively relative to baseline (Fig. 3a).

Tumor v_e of 2 and 10 tumors on day 1, 5 and 6 tumors on visit 2, and 2 and 0 tumors in the last visit, were below –RC and above +RC, respectively relative to baseline (Fig. 3b).

Tumor v_p of 4 and 12 tumors on day 1, 7 and 11 tumors on visit 2, and 1 tumor each at the last visit, were below –RC and above +RC respectively relative to baseline (Fig. 3c).

Similar results were obtained per patient considering if at least one tumor was either below –RC or above +RC. More patients had changes below –RC than above +RC for ADC and T1, and above +RC in the other parameters (see Supplementary Table 2).

Reproducibility of median ADC, T1, iAUC, k^{trans} , v_e and v_p in multiple normal tissues (muscle, liver, spleen, renal cortex, adipose tissue) across patients and scan dates is presented in Supplementary Fig. 3.

The results in Figs. 1, 2, 3 suggest a response to PEGPH20 treatment that manifests as a decrease in ADC and T1 on day 1, possibly from a decrease in tumor extracellular water content due to HA depletion²⁰. Results

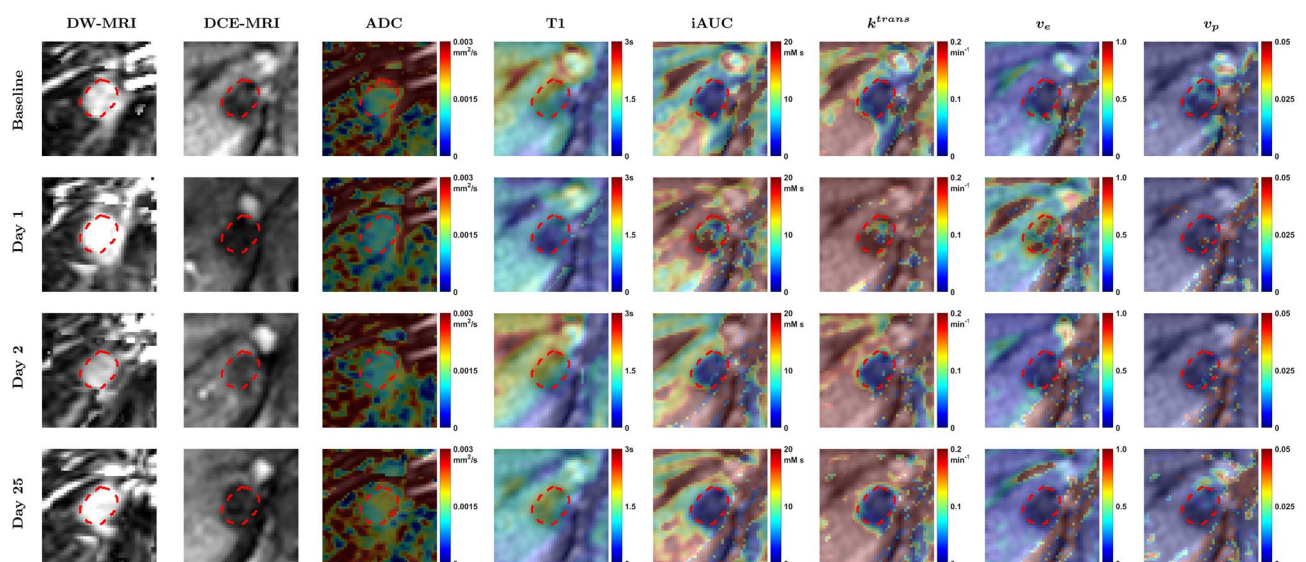


Figure 1. DW-MRI ($b = 0 \text{ s}/\text{mm}^2$), DCE-MRI images (2nd time point after AIF peak), and parameter maps per visit of a metastatic colorectal cancer tumor located in the liver of patient 102-003-105 (tumor 2). Contour annotation of tumor is shown as dashed red line. After PEGPH20 (Day 1) a decrease in ADC and T1, and an increase in iAUC, k^{trans} , and v_e within the tumor are observed. An increase in v_p is observed in few pixels.

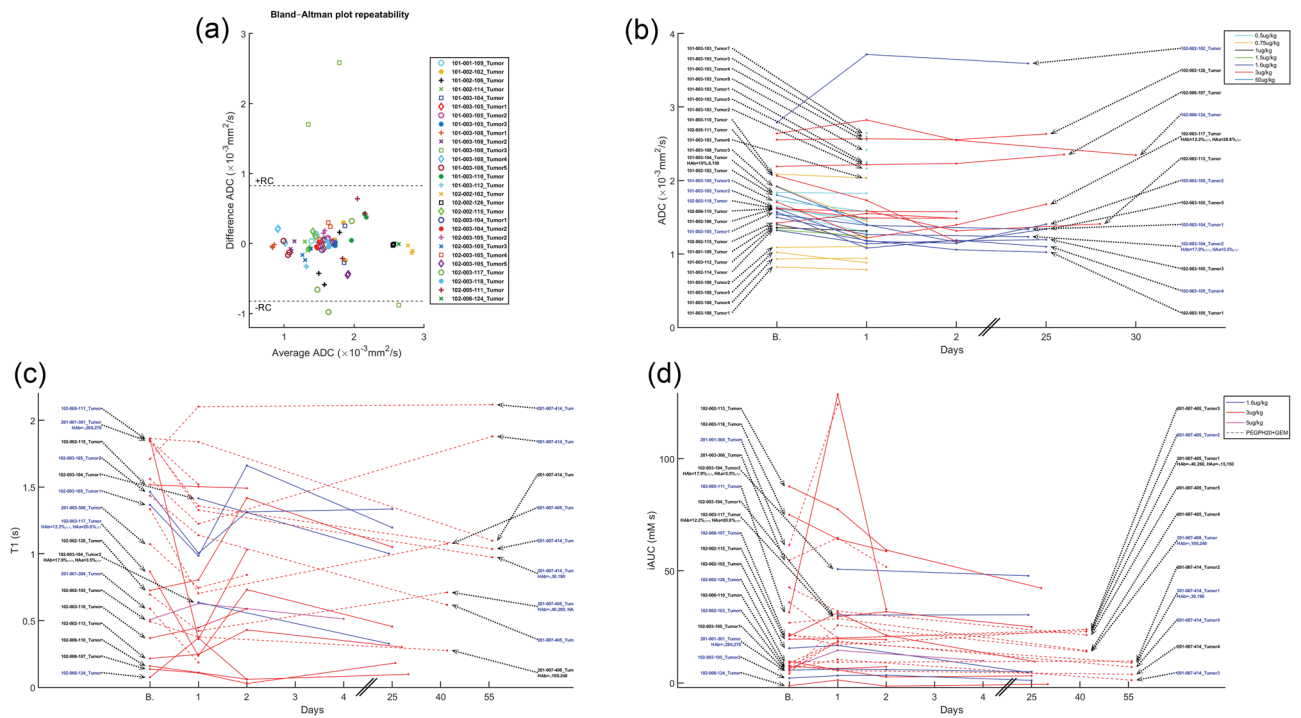


Figure 2. Median parameter changes at each time point for each tumor. In all parameter change figures, the patient/lesionID in blue indicates a true significant change on Day 1 based on the RC. In the x-axes, “B” indicates the baseline time point. In patients with available HA levels, HAB is the baseline HA level (HA%, tumor, and stroma H-score) and HAa is the post-PEGPH20 HA level. In ADC, where repeated scans were available, Bland–Altman plot describing median ADC repeatability is also shown, where each marker/color represents a baseline ADC replicate difference.

also show an increase in $iAUC$, k^{trans} , and v_p on day 1, suggesting an increase in perfusion, permeability, and vascularity. v_e also increased after treatment, suggesting a release of ECM space.

Pairs of median parameter changes (Day 1 – Baseline) that were significantly correlated are shown in Fig. 4 (bottom row); whereas changes in ADC and T1 are significantly correlated to one another, changes in v_e are correlated with changes in most other parameters.

Scatter plots of median parameter changes (Day 1 – Baseline) vs. their baseline values are shown in Fig. 4 (top row). Most points in ΔADC and $\Delta T1$ are negative, confirming the tendency of ADC and T1 to decrease following PEGPH20 treatment. Also, there is a negative correlation, which suggests a dependency of response to baseline values. Significant changes in ADC and T1 below –RC are more likely in tumors with baseline ADC values above $1.46 \times 10^{-3} \text{ mm}^2/\text{s}$ and baseline T1 values above 0.54 s. These thresholds are defined to maximize sensitivity and specificity. Balanced Accuracy using these thresholds for both ADC and T1 are 72% and 82%.

Most changes in the other parameters are positive on day 1 (Fig. 4). For $iAUC$, there is a negative correlation to baseline values with most significant changes above +RC happening in tumors with baseline values below 9.2 $\text{mM}\cdot\text{s}$ (BA = 76%). Changes in v_e and v_p are also negatively correlated to baseline, with thresholds to separate significant and non-significant changes above +RC at 0.17 (BA = 68%) and 0.02 (BA = 60%) respectively. Changes in k^{trans} trended negatively with respect to baseline values though this relationship was not statistically significant (optimal threshold 0.07 min^{-1} , BA = 72%, $p > 0.05$).

No clear relation was observed between changes in quantitative MRI parameters and drug dose or drug pharmacokinetics (C_{max} , C_{min} , AUC). Also, no relation was observed with HA levels in stained tumors and survival (Supplementary Tables 3, 4, 5).

To investigate the robustness of the results with respect to the manual annotations, an expert radiologist (JRC) re-annotated tumors in a subset of five patients on DW-MRI and DCE-MRI at each visit. Correlations of median tumor parameters between observers are shown in Fig. 5, revealing very high correlations ($ICC \sim 0.9$).

Pixel-wise analysis

A pixel-wise analysis of all parameter values was carried out to develop a multivariable model for predicting post-PEGPH20 response in any parameter from baseline parameter values. Eleven patients have lesions imaged using DWI, T1, and DCE-MRI; however, in three patients either ADC, T1 or DCE parameters could not be computed at baseline; and in two patients (102-002-115, 102-002-126) the sequences were not all acquired in the same view. In all, it was possible to co-register DWI, T1, and DCE-MRI sequences across scan dates in six patients, as shown for one patient in Fig. 1, and these were used in the pixel-wise analysis. Parameter changes in pixels from these six patients between Day 1 and baseline were visualized using Principal Component Analysis

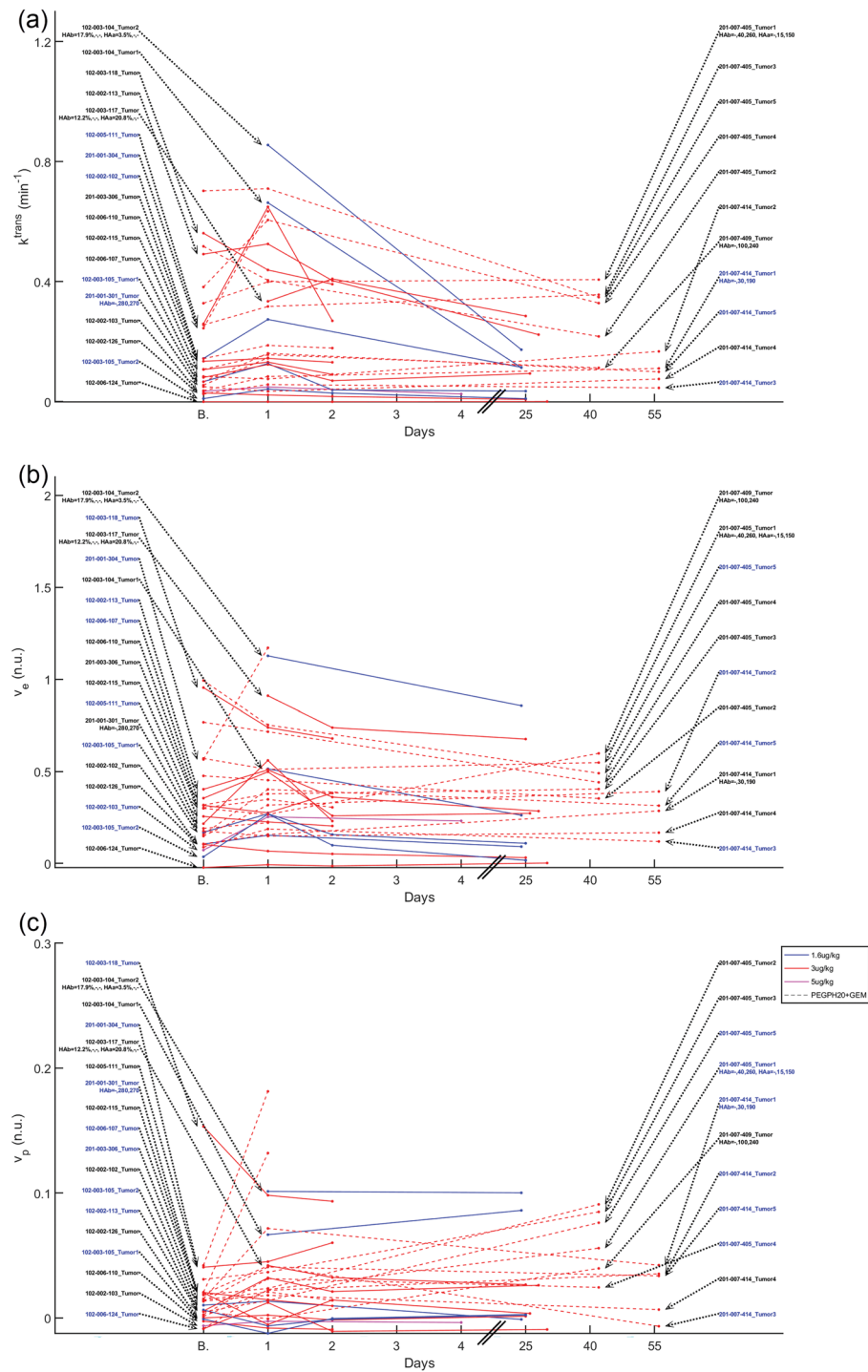


Figure 3. Median parameter changes at each time point for each tumor. In all parameter change figures, the patient/lesionID in blue indicates a true significant change on Day 1 based on the RC. In the x-axes, “B.” indicates the baseline time point. In patients with available HA levels, HAB is the baseline HA level (HA%, tumor, and stroma H-score) and HAa is the post-PEGPH20 HA level.

(PCA) to identify two clusters (Supplementary Fig. 4). As in the VOI analysis, each tumor pixel was considered to either be a pharmacodynamic responder (p-responder) or non-responder (p-non-responder) based on its parameter changes relative to its RC.

For ADC we applied the pixelwise RC per tumor when baseline repeats were available, or otherwise the group pixel-wise $RC = 1.4 \times 10^{-3} \text{ mm}^2/\text{s}$ obtained from all patients using equal numbers of pixels per patient. For the other parameters we used the same RC as in the VOI analysis. A pixel with a parameter change between Day 1 and

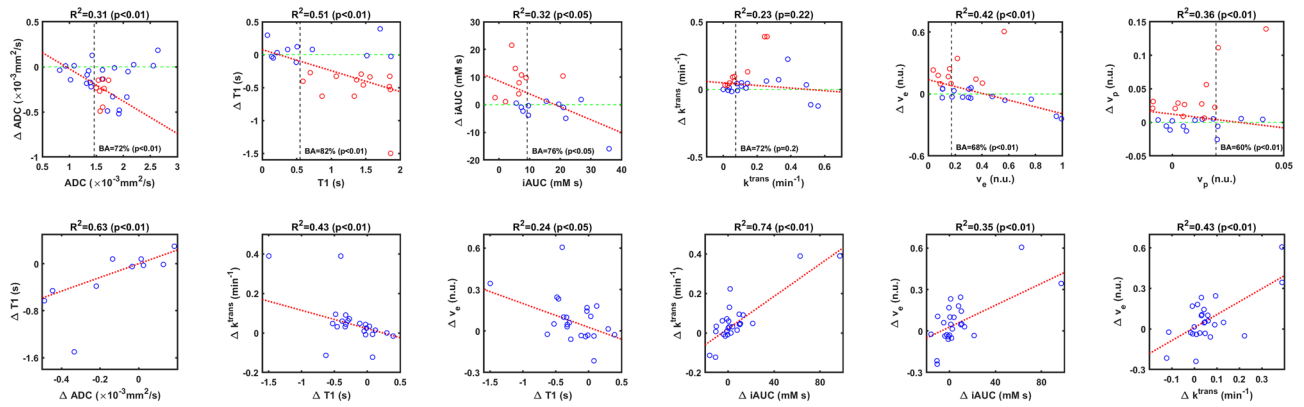


Figure 4. Top Row: Scatter plots of median parameter changes (Δ Parameter = Parameter Value at Day 1 – Parameter Value at Baseline) vs. their baseline values. Red circles indicate significant changes below $-RC$ for ADC and T1, and above $+RC$ otherwise. A linear regression is shown in red dotted line (its R^2 and p -value (F-test) are above each plot). The vertical dotted black line indicates the threshold that maximizes BA for significant changes at day 1. BA and its p -value (McNemar test) are also shown. Bottom Row: pairs of median parameter changes (Day 1 – Baseline) that are significantly correlated. Some outliers are not shown to improve visualization.

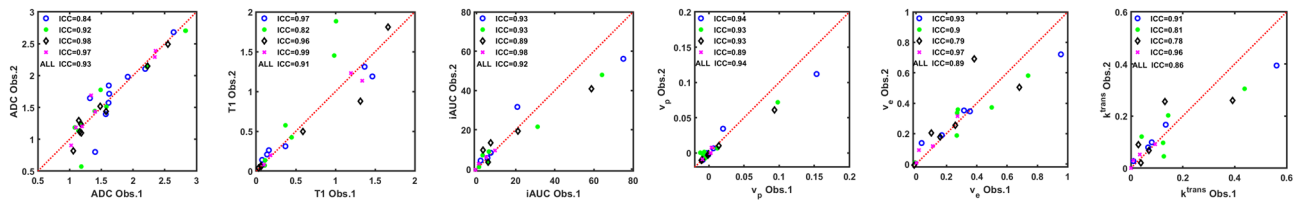


Figure 5. Inter-observer variability analysis. Each point represents a median parameter for each tumor annotated by observer 1 (NR) and observer 2 (JRC) on a subset of 5 patients (102–003–105, 102–003–118, 102–006–107, 102–006–110, 102–006–124). Blue circles are the baseline values, green * are the day 1 values, black diamonds are the visit 2 values, and purple × are the last visit. Intra-class correlations (ICC) for each visit and all points are depicted. Units are $\times 10^{-3}$ mm^2/s for ADC, s for T1, $\text{mM}\cdot\text{s}$ for iAUC, min^{-1} for k^{trans} , while both v_e and v_p are dimensionless.

baseline that is below $-RC$ for ADC and T1, or above $+RC$ for the other parameters, was labeled a “p-responder” pixel, and otherwise a “p-non-responder” pixel.

Using the pixelwise baseline parameter values as independent variables and the pixel class (p-responder or p-non-responder) as the dependent variable, we trained a decision tree model using the machine learning software Weka (www.cms.waikato.ac.nz/ml/weka/). To mitigate model over-fitting, we separated pixels into two sets, one for training and one for validation. To avoid biasing results towards larger tumors with more pixels, during the training process we sampled an equal number of pixels per patient, equivalent to 85% pixels from the smallest tumor, with the remaining pixels used for validation. Additionally, to avoid problems with unbalanced data, the sampling process during model training was randomized to select equal numbers of “p-responder” and “p-non-responder” in the training set. After each training iteration, the resulting decision tree was applied to the validation set, and a BA per patient was obtained; this process was repeated multiple times with random sampling from the six patients. After this process, the optimal model (maximum BA in the validation set) was a simple rule: pixels with baseline $v_e < 0.39$ are predicted to be “p-responder”, and otherwise predicted to be “p-non-responder” (average BA = 74.4% in the validation set, average training BA = 69.2%). As each patient contributed data to the training and validation sets, we performed a leave-one-patient-out cross-validation, obtaining an evaluation average BA = 65.6% across patients (Supplementary Table 6).

Discussion

Pre-clinical studies proved that PEGPH20 successfully depletes intratumoral HA^{2,4,7–9,11}, resulting in higher concentrations of concomitant chemotherapies in experimental tumors^{7,9}. These results led to clinical studies where, despite early success in phase I/II studies showing survival benefits^{6,12,13}, follow-up phase II/III studies failed to show improved outcomes for patients treated with PEGPH20 vs. placebo^{14,15}. Reasons for these failures include either failure to pre-select patients¹⁵, or pre-selection of patients with oligometastatic disease using the HA status of only a single tumor¹⁴. These failures also underscore the need for improved understanding of tumor stroma remodeling following PEGPH20 treatment¹⁴. In this work we have sought to address both these needs by investigating post-PEGPH20 changes in the tumor microenvironment using qMRI, and identifying qMRI parameters for informing patient pre-selection. First, we analyzed changes of several tumor properties measured

by qMRI, namely, ADC, T1, iAUC, k^{trans} , v_e , and v_p , from patients enrolled in three early-phase clinical studies of PEGPH20. Second, we present a pharmacodynamic response predictor that could potentially be useful as a MRI biomarker to pre-select patients who are good candidates for combination chemotherapy with PEGPH20.

There was unavoidable heterogeneity of tumor types and locations in these early-phase drug development studies, notwithstanding which some quantitative findings were discernible. Tumors that were treated with PEGPH20 exhibited an acute decrease in ADC and T1, and these decreases were correlated with each other. This finding is consistent with pre-clinical reports of post-PEGPH20 decrease of ADC in breast tumors^{20,22} and decrease of extracellular water content in pancreatic tumors². A post-PEGPH20 decrease in ADC was also reported in a preliminary analysis of clinical data²¹. A decrease in ADC and T1 suggests a decrease in extracellular water due to HA depletion after PEGPH20, as shown by DuFort et al.². A post-PEGPH20 increase in iAUC, k^{trans} , v_e , and v_p was also observed in tumors in our study. Post-PEGPH20 increase in tumor k^{trans} has previously been reported in pre-clinical studies⁹ and in a clinical study of a limited subset of patients^{5,6}. A decrease in HA could release tumor interstitial pressure, resulting in increased vascular space causing a higher v_p , resulting in a higher blood flow manifesting as increased iAUC and k^{trans} . Depletion of HA would release ECM space, which would manifest as increase in v_e . Also, this increased v_e and v_p could suggest a decrease in IFP. We observed most parameter changes to be significantly correlated to changes in v_e , indicating that a change in v_e is the most relevant early response biomarker and tumor property that triggers other changes such as the increase in tumor perfusion and permeability, something that was also confirmed in the pixel-wise analysis where a low v_e at baseline was predictive of response in any parameter.

A change in any MRI-measured parameter was considered significant if the median change was outside the RC, a measure of parameter variability in repeated scans. For ADC, in most cases an RC per tumor was obtained from repeated scans acquired at baseline. For other parameters, we used literature RC values since repeated T1w-MRI and DCE-MRI scans were not available. A decrease of ADC and T1 below $-RC$, and an increase in iAUC, k^{trans} , v_e , and v_p above $+RC$, at Day1 post-PEGPH20 relative to baseline values, were considered a pharmacodynamic response to treatment with PEGPH20. This approach could be used at follow-up to determine if a patient is responding to PEGPH20.

We did not observe correlations between parameter changes and either changes in HA or survival, though such analyses were limited by only a few biopsied tumors and good responders by RECIST criteria that were available in our data set. qMRI parameter changes also did not correlate with PEGPH20 dose, which is unsurprising since PEGPH20 is an enzyme and therefore dose–response would not be characterized by the Law of Mass Action.

QIBA recommendations for the high b value are 500–600 s/mm² or higher for abdominal, pelvic, breast and brain DW-MRI, and $b < 100$ s/mm² for the lowest b value^{29,33}. We fixed two b values (0 and 450 s/mm²) in the imaging manual as a compromise between QIBA recommendations and signal-to-noise ratio in the expected diversity of metastatic tumor locations (chest, lung, abdominal and pelvic lesions) in these early-phase studies. DCE-MRI indicated increased post-PEGPH20 tumor perfusion. The choice of low b value of 0 s/mm² could lead to higher calculated values of ADC due to the confounding effects of perfusion, but we measured decreases in post-PEGPH20 tumor ADC values, suggesting that DW-MRI and DCE-MRI measurements report on distinct and independent changes within PEGPH20-treated tumors.

We identified threshold values of each parameter at baseline for predicting pharmacodynamic response. Baseline parameter values that maximized sensitivity and specificity for prediction of response to PEGPH20 were: $ADC > 1.46 \times 10^{-3}$ mm²/s, $T1 > 0.54$ s, $iAUC < 9.2$ mM s, $k^{trans} < 0.07$ min⁻¹, $v_e < 0.17$, and $v_p < 0.02$. These relations produce significant accuracies above 70% in most cases. High ADC would be expected in tumor regions with high extracellular water content²³ such as would be associated with tumor HA. High extracellular water content would also be associated with longer tumor T1 values. Low iAUC and k^{trans} suggest low perfusion and permeability, while low v_p indicates low vascularity such as might be the case in tumor microenvironments with microvascular compression due to high interstitial pressures stemming from high HA. A low v_e indicates a small ECM space likely due to high HA. Baseline values of these parameters can be used to pre-select patients with tumors that are likely to respond to PEGPH20, and would therefore experience improved tumor penetration by intravenously administered small molecule chemotherapeutics upon pre-treatment or co-treatment with PEGPH20. In this context, our results indicate that tumor pixels with $v_e < 0.39$ at baseline are more likely to exhibit favorable post-PEGPH20 changes in DW-MRI and DCE-MRI metrics, including perfusion-related parameters. A caveat is that this baseline predictor was identified on retrospective analysis of data acquired in a heterogeneous population of patients and tumor types, and requires prospective validation in a follow-up study.

Another caveat is that we utilized volumetric RC rather than a pixelwise RC for analysis of DCE-MRI parameters, which may have resulted in overestimate of the fraction of p-responder pixels in the tumors we analyzed. Also, in pixel-wise analysis we did not consider the impact of changes in gross tumor morphology and size between visits, which could lead to misregistration at the pixel level.

In a limited repeatability analysis, we also observed that tumor parameter values were highly correlated between tumor annotations independently made by two observers.

In summary, our DW-MRI and DCE-MRI studies indicate that treatment with PEGPH20 produces a release of extracellular/interstitial water along with improved penetration of the tumor by intravenously administered small molecule gadolinium-based MRI contrast agent. We have identified MRI biomarkers to guide the pre-selection of patients, and for non-invasively monitoring tumor response to co-treatment with PEGPH20. Elevated tumor HA correlates with poorer prognosis in several cancers besides PDA, such as breast, gastric, colorectal, ovarian, prostate, and lung¹². We enthusiastically look forward to the results of new and emerging studies of PEGPH20 where treatment has previously been shown to be well tolerated³⁴. We believe that future clinical trials of PEGPH20 and other stromal modifiers should incorporate acquisition of quantitative MRI, and anticipate that the predictive and prognostic MRI biomarkers presented here will inform these future studies.

Data availability

The raw data used in the current study are available from the corresponding author upon reasonable request and with permission of Halozyne Therapeutics. Complete results from the reported analyses are shared as per-patient HTML reports that depict all slices of raw qMRI images, processed qMRI images, and computed maps of ADC, T1, iAUC, k^{trans} , v_p , and v_e from all scan dates of each subject, in the following repository: <https://www.kaggle.com/datasets/natarajanraghunand/mri-in-pegph20-early-phase-clinical-trials>. MATLAB code for reproducing the image processing in this study is shared here: <https://github.com/xandresariasx/ADC-and-perfusion-parameters-from-MRI/>

Received: 31 August 2023; Accepted: 17 May 2024

Published online: 21 May 2024

References

- Provenzano, P. P. & Hingorani, S. R. Hyaluronan, fluid pressure, and stromal resistance in pancreas cancer. *Br. J. Cancer* **108**, 1–8. <https://doi.org/10.1038/bjc.2012.569> (2013).
- DuFort, C. C. *et al.* Interstitial pressure in pancreatic ductal adenocarcinoma is dominated by a gel-fluid phase. *Biophys. J.* **110**, 2106–2119. <https://doi.org/10.1016/j.bpj.2016.03.040> (2016).
- DuFort, C. C., DelGiorno, K. E. & Hingorani, S. R. Mounting pressure in the microenvironment: Fluids, solids, and cells in pancreatic ductal adenocarcinoma. *Gastroenterology* **150**, 1545–1557.e1542. <https://doi.org/10.1053/j.gastro.2016.03.040> (2016).
- Li, X. *et al.* Parallel accumulation of tumor hyaluronan, collagen, and other drivers of tumor progression. *Clin. Cancer Res.* **24**, 4798–4807. <https://doi.org/10.1158/1078-0432.Ccr-17-3284> (2018).
- Infante, J. R. *et al.* Phase 1 trials of PEGylated recombinant human hyaluronidase PH20 in patients with advanced solid tumours. *Br. J. Cancer* **118**, 153–161. <https://doi.org/10.1038/bjc.2017.327> (2018).
- Hingorani, S. R. *et al.* Phase Ib study of PEGylated recombinant human hyaluronidase and gemcitabine in patients with advanced pancreatic cancer. *Clin. Cancer Res.* **22**, 2848–2854. <https://doi.org/10.1158/1078-0432.Ccr-15-2010> (2016).
- Thompson, C. B. *et al.* Enzymatic depletion of tumor hyaluronan induces antitumor responses in preclinical animal models. *Mol. Cancer Therap.* **9**, 3052–3064. <https://doi.org/10.1158/1535-7163.Mct-10-0470> (2010).
- Maloney, E. *et al.* Non-invasive monitoring of stromal biophysics with targeted depletion of hyaluronan in pancreatic ductal adenocarcinoma. *Cancers (Basel)* **11**, 772. <https://doi.org/10.3390/cancers11060772> (2019).
- Cao, J. *et al.* Dynamic contrast-enhanced MRI detects responses to stroma-directed therapy in mouse models of pancreatic ductal adenocarcinoma. *Clin. Cancer Res.* **25**, 2314–2322. <https://doi.org/10.1158/1078-0432.CCR-18-2276> (2019).
- Provenzano, P. P. *et al.* Enzymatic targeting of the stroma ablates physical barriers to treatment of pancreatic ductal adenocarcinoma. *Cancer Cell* **21**, 418–429. <https://doi.org/10.1016/j.ccr.2012.01.007> (2012).
- Jacobetz, M. A. *et al.* Hyaluronan impairs vascular function and drug delivery in a mouse model of pancreatic cancer. *Gut* **62**, 112–120. <https://doi.org/10.1136/gutjnl-2012-302529> (2013).
- Wong, K. M., Horton, K. J., Coveler, A. L., Hingorani, S. R. & Harris, W. P. Targeting the tumor stroma: The biology and clinical development of pegylated recombinant human hyaluronidase (PEGPH20). *Curr. Oncol. Rep.* **19**, 47. <https://doi.org/10.1007/s11912-017-0608-3> (2017).
- Hingorani, S. R. *et al.* HALO 202: Randomized phase II study of PEGPH20 plus nab-paclitaxel/gemcitabine versus nab-paclitaxel/gemcitabine in patients with untreated, metastatic pancreatic ductal adenocarcinoma. *J. Clin. Oncol.* **36**, 359–366. <https://doi.org/10.1200/jco.2017.74.9564> (2018).
- Van Cutsem, E. *et al.* Randomized phase III trial of pegvorhyaluronidase alfa with nab-paclitaxel plus gemcitabine for patients with hyaluronan-high metastatic pancreatic adenocarcinoma. *J. Clin. Oncol.* **38**, 3185–3194 (2020).
- Ramanathan, R. K. *et al.* Phase IB/II randomized study of FOLFIRINOX plus pegylated recombinant human hyaluronidase versus FOLFIRINOX alone in patients with metastatic pancreatic adenocarcinoma: SWOG S1313. *J. Clin. Oncol.* **37**, 1062–1069 (2019).
- Hosein, A. N., Brekken, R.A.-O. & Maitra, A.A.-O. Pancreatic cancer stroma: An update on therapeutic targeting strategies. *Nat. Rev. Gastroenterol. Hepatol.* **17**, 487–505 (2020).
- Hakim, N., Patel, R., Devoe, C. & Saif, M. W. Why HALO 301 failed and implications for treatment of pancreatic cancer. *Pancreas* **3**, e1–e4 (2020).
- Gebauer, F., Kemper, M., Sauter, G., Prehm, P. & Schumacher, U. Is hyaluronan deposition in the stroma of pancreatic ductal adenocarcinoma of prognostic significance?. *PLoS One* **12**, e0178703. <https://doi.org/10.1371/journal.pone.0178703> (2017).
- Whattcott, C. J. *et al.* Desmoplasia in primary tumors and metastatic lesions of pancreatic cancer. *Clin. Cancer Res.* **21**, 3561–3568. <https://doi.org/10.1158/1078-0432.Ccr-14-1051> (2015).
- Reeves, E. L. *et al.* Breast tumour response to PEGPH20-induced stromal modulation assessed by multiparametric MRI. *Proc. ISMRM* **3**, 043 (2020).
- Arias Lorza, A. M. & Raghunand, N. ADC decreases in solid tumors following monotherapy with pegylated recombinant human hyaluronidase: Results from early-phase clinical trials. *Proc. ISMRM* **5**, 0949 (2021).
- Reeves, E. L. *et al.* Investigating the contribution of hyaluronan to the breast tumour microenvironment using multiparametric MRI and MR elastography. *Mol. Oncol.* **17**, 1076–1092. <https://doi.org/10.1002/1878-0261.13437> (2023).
- Chenevert, T. L. *et al.* Diffusion coefficient measurement using a temperature-controlled fluid for quality control in multicenter studies. *J. Magn. Reson. Imaging* **34**, 983–987. <https://doi.org/10.1002/jmri.22363> (2011).
- Malyarenko, D. *et al.* Multi-system repeatability and reproducibility of apparent diffusion coefficient measurement using an ice-water phantom. *J. Magn. Reson. Imaging* **37**, 1238–1246. <https://doi.org/10.1002/jmri.23825> (2013).
- Arias Lorza, A. M. *et al.* Dose–response assessment by quantitative MRI in a phase I clinical study of the anti-cancer vascular disrupting agent crolibulin. *Sci. Rep.* **10**, 14449. <https://doi.org/10.1038/s41598-020-71246-w> (2020).
- Sandmann, C., Hodneland, E. & Modersitzki, J. A practical guideline for T1 reconstruction from various flip angles in MRI. *J. Algorithms Comput. Technol.* **10**, 213–223. <https://doi.org/10.1177/1748301816656288> (2016).
- Pineda, F. D., Medved, M., Fan, X. & Karczmar, G. S. B1 and T1 mapping of the breast with a reference tissue method. *Magn. Reson. Med.* **75**, 1565–1573 (2016).
- Shen, Y. *et al.* T1 relaxivities of gadolinium-based magnetic resonance contrast agents in human whole blood at 15, 3, and 7 T. *Investig. Radiol.* **50**, 330–338. <https://doi.org/10.1097/rli.000000000000132> (2015).
- Shukla-Dave, A. *et al.* Quantitative imaging biomarkers alliance (QIBA) recommendations for improved precision of DWI and DCE-MRI derived biomarkers in multicenter oncology trials. *J. Magn. Reson. Imaging* **49**, e101–e121 (2019).
- McHugh, D.A.-O. *et al.* Image contrast, image pre-processing, and T(1) mapping affect MRI radiomic feature repeatability in patients with colorectal cancer liver metastases. *Cancers (Basel)* **13**, 240 (2021).
- Galbraith, S. M. *et al.* Reproducibility of dynamic contrast-enhanced MRI in human muscle and tumours: Comparison of quantitative and semi-quantitative analysis. *NMR Biomed.* **15**, 132–142 (2002).

32. Yang, C. *et al.* Reproducibility assessment of a multiple reference tissue method for quantitative dynamic contrast enhanced-MRI analysis. *Magn. Reson. Med.* **61**, 851–859 (2009).
33. Padhani, A. R. *et al.* Diffusion-weighted magnetic resonance imaging as a cancer biomarker: Consensus and recommendations. *Neoplasia (New York, N.Y.)* **11**, 102–125. <https://doi.org/10.1593/neo.81328> (2009).
34. Heineman, T. *et al.* Safety and pharmacokinetics of docetaxel in combination with pegvorhyaluronidase alfa in patients with non-small cell lung cancer. *Clin. Transl. Sci.* **14**, 1875–1885 (2021).

Acknowledgements

The authors thank all patients involved in the study, as well as their caregivers, care team, investigators, and research staff.

Author contributions

A.M.A.-L.: Software, Formal analysis, Methodology, Writing-original draft, Writing-review and editing. J.R.C.: Formal analysis, Writing-review and editing. S.R.H.: Data Curation, Writing-review and editing. D.D. V.H.: Data Curation, Writing-review and editing. R.L.K.: Resources, Data Curation, Project Administration, Writing-review and editing. N.R.: Conceptualization, Resources, Data Curation, Software, Formal analysis, Supervision, Funding Acquisition, Methodology, Writing-original draft, Project Administration, Writing-review and editing.

Funding

This study was partly supported by a research grant from Halozyme Therapeutics to NR, and by the National Institutes of Health to NR (P30 CA076292, Quantitative Imaging Core).

Competing interests

NR received a research grant from Halozyme Therapeutics for the work reported here. SRH and DDVH received funding to their institutions from Halozyme to defray study-related costs. RLK is Founder and CEO of Imaging Endpoints, LLC. No potential conflicts of interest were disclosed by the other authors. The data analyses reported here remained under the full control of the authors.

Additional information

Supplementary Information The online version contains supplementary material available at <https://doi.org/10.1038/s41598-024-62470-9>.

Correspondence and requests for materials should be addressed to N.R.

Reprints and permissions information is available at www.nature.com/reprints.

Publisher's note Springer Nature remains neutral with regard to jurisdictional claims in published maps and institutional affiliations.



Open Access This article is licensed under a Creative Commons Attribution 4.0 International License, which permits use, sharing, adaptation, distribution and reproduction in any medium or format, as long as you give appropriate credit to the original author(s) and the source, provide a link to the Creative Commons licence, and indicate if changes were made. The images or other third party material in this article are included in the article's Creative Commons licence, unless indicated otherwise in a credit line to the material. If material is not included in the article's Creative Commons licence and your intended use is not permitted by statutory regulation or exceeds the permitted use, you will need to obtain permission directly from the copyright holder. To view a copy of this licence, visit <http://creativecommons.org/licenses/by/4.0/>.

© The Author(s) 2024